# UC Irvine
## UC Irvine Previously Published Works

**Title**

Observational Signatures of Gamma Rays from Bright Blazars and Wakefield Theory

**Permalink**

https://escholarship.org/uc/item/14g9m3xg

**Journal**

Monthly Notices of the Royal Astronomical Society, 493(2)

**ISSN**

0035-8711

**Authors**

Canac, NE
Abazajian, KN
Tajima, T
et al.

**Publication Date**

2020-04-01

**DOI**

10.1093/mnras/staa338

Peer reviewed

# OBSERVATIONAL SIGNATURES OF GAMMA RAYS FROM BRIGHT BLAZARS AND WAKEFIELD THEORY

N. E. Canac[1], K. N. Abazajian[1], T. Tajima[1], T. Ebisuzaki[2] and S. Horiuchi[3]
*Draft version April 30, 2019*

## ABSTRACT

Gamma-ray observations have revealed strong variability in blazar luminosities in the gamma-ray band over time scales as short as minutes. We show, for the first time, that the correlation of the spectrum with intensity is consistent with the behavior of the luminosity variation of blazar SEDs along a blazar sequence for low synchrotron peak blazars. We show that the observational signatures of variability with flux are consistent with wakefield acceleration of electrons initiated by instabilities in the blazar accretion disk. This mechanism reproduces the observed time variations as short as 100 seconds. The wakefield mechanism also predicts a reduction of the electron spectral index with increased gamma-ray luminosity, which could be detected in higher energy observations well above the inverse Compton peak.

## 1. INTRODUCTION

Bright gamma-ray emitting blazars have been detected to have variability in flux by a factor of two and more on time scales from minutes to weeks (Albert et al. 2007; Aharonian 2007; Aleksic et al. 2011; Abdo et al. 2010b,a). This short-scale temporal variability has presented a strong challenge to jet emission models. The spectral indices are often also time variable, around the index of two or greater (Abdo et al. 2010b; Albert et al. 2007; Chen et al. 2013). Furthermore, an anti-correlation of the spectral index and the gamma-ray flux is also reported (Abdo et al. 2010b), which implies a connection to the underlying emission mechanism. The High Energy Stereoscopic System (HESS) telescope has observed flares on time scales of ∼200 seconds in Very High Energy (VHE) > 100 GeV gamma rays with peak fluxes at a factor of two above the average flux toward the blazar PKS 2155-304 (Aharonian 2007). The MAGIC telescope has seen flux variability by an order of magnitude over several minutes, with a hardening of the spectrum (corresponding to lower spectral index) with increasing flux (Albert et al. 2007). Similar variation is seen in PKS 1222+21 in VHE observations by MAGIC, with a potential smooth spectral connection to the GeV scale in observations by the Large Area Telescope *Fermi Gamma Ray Space Telescope* (Fermi-LAT) (Aleksic et al. 2011).

The lack of a strong spectral break in the VHE gamma rays has indicated that the jet emission mechanism must be outside of the broad-line emission region (BLR), i.e., away from the region's very high photon densities. From the temporal variability it can be inferred that the emission region must be very compact, of order $\sim 10^{14}$ cm from causality. To avoid the optical depth within the BLR region, it has been hypothesized that there are small-scale regions embedded within a larger jet (e.g., Giannios et al. 2009). Accommodating these phenomena in traditional jet emission models has proved so challenging, as to motivate new axion-like-particles to allow for photon-axion mixing to potentially provide the temporal variability and spectral features (e.g., Tavecchio et al. 2012). Alternatively, studies have tied the timescales of episodic emission in the magnetic field of the jet (Marscher et al. 2008) with optical variability (Edelson et al. 2013, 2014).

Fermi-LAT observations have revealed GeV gamma-ray signatures from the brightest blazars (Abdo et al. 2010b). Notably the gamma-ray observations from Blazar AO 0235+164 and 3C 454.3 show similar properties such as:

1. The photon index is around 2 or slightly above 2 in their respective lowest value;

2. the photon index varies rapidly from its lowest (around 2) to highest (around 2.8 or so) value over a period of several weeks;

3. the luminosity (flux) of the gamma rays also varies rapidly over the same time period of several weeks, by as much as a factor of five;

4. and, most importantly, the luminosity peak and the valley (hardening) of the photon index positively coincide. In other words, the time variations of the photon index and luminosity faithfully anti-correlate. This anti-correlation clearly persists regardless of different periods from hundreds of seconds to months, demonstrating a remarkable universality in the phenomenon.

We show in this paper, for the first time, that the rapid variations of high-energy gamma emissions and the strong anti-correlation between the luminosity and photon index is consistent with a blazar SED sequence shift. We further show that the timing of the variations is consistent with magneto-rotational episodic instabilities, recently studied in Mizuta et al. (2017). We show that the inherent acceleration mechanism may be probed by further analysis of the highest energy blazar spectra and their variability.

In Section 2, we review the theory of wakefield acceleration, and in Section 3, we review the gamma-ray emission processes relevant for the wakefield acceleration mechanism in the context of blazars. In Section 4, we detail

[1] Department of Physics and Astronomy, University of California, Irvine, Irvine, California 92697, USA
[2] RIKEN, Wako, Saitama, Japan
[3] Center for Neutrino Physics, Department of Physics, Virginia Tech, Blacksburg, VA 24061, USA

our gamma-ray analysis setup, and present our results in Section 5. We conclude in Section 6.

## 2. MAGNETO-ROTATIONAL INSTABILITY AND WAKEFIELD ACCELERATION

As a theory for the underlying electron energy injection, ponderomotive acceleration provides a theoretical framework of the extremely relativistic collective acceleration mechanism in an idealized case (Ebisuzaki & Tajima 2014a,b). In this mechanism, the wave front is regarded as one-dimensional only depending on the coordinate in the direction of the Alfven shock (and its mode-converted electromagnetic (EM)) waves along the jet propagation. In this one-dimensional model the coherence of high energy acceleration is guaranteed with the asymptotically tending velocity of the EM group velocity being the speed of light $c$ (Tajima & Dawson 1979; Ashour-Abdalla et al. 1981). This is best realized when the pulse contains a single frequency carrier EM wave (just as is the case of a laboratory laser experiment). This may not be necessarily the case in our astrophysical setting, in which we expect a multiple set of frequencies of EM waves. However, we note that the group velocities of various EM waves with different frequencies are nearly equal to $c$ in the one-dimensional case. Furthermore, as explained in the theory of Ebisuzaki & Tajima (2014a), the pulse is generated by the striking of an acceleration of matter ejected by a major disruption of the AGN accretion disk. As such, an eruption could be represented by one major bang (though could be a series of such) which results in a predominance of a single pulse with a typical length of the disk thickness. This results in the following situation: while the accelerating field acquires a complex phase structure, the phase velocity of each portion of the wave substructure is again close to $c$, i.e., $c\sqrt{(1 - \omega_p^2/\omega(z)^2)}$, where $\omega(z)$ is the frequency of that local, where $z$ is along the jet propagation and substructure's frequency and $\omega_p$ is the plasma frequency where the pulse propagates. This mechanism is one of the origins of relativistic coherence, as pointed out in Tajima (2010).

While the relativistic coherence is preserved in the one-dimensional situation, the de-trapping of particles in this multi-frequency EM drive becomes much more frequent than that of a single carrier case. This incessant de-trapping (and subsequent re-trapping and its repetition of these processes) gives rise to the emergence of phase-induced stochasticity (Mima et al. 1991). According to this theory, the resultant energy spectrum in one-dimension takes $E^{-2}$, i.e., the energy spectral index of 2. That is, in the most ideal situation of purely one-dimensional ponderomotive acceleration, the energy spectrum takes index of 2. In less idealistic cases of two-dimensions (or three-dimensions), the ponderomotive acceleration incurred by waves that point to various directions (albeit within a narrow cone around the jet direction $z$) now makes the de-trapping more rapid so that the accelerating length per one episode of the wave trapping of particles becomes shortened and the energy gain less. We call this as the shortening of the de-phasing length as a function of the dimensions of the wave structure (Tajima & Dawson 1979). This leads to an energy spectral index greater than 2, with more particles dominating in lower energy bracket. If we compare the first one-dimensional case with the two-dimensional (three-dimensions) case, the amount of energy gain is higher in one-dimension than in two-dimensions, as more coherent energy gain is realized in the former. Thus it is this intrinsic mechanism of the ponderomotive acceleration that makes the lower index case acquire greater and more coherent energy gain in one-dimension than the cases in more spread wave propagation in two-dimensional (and three-dimensional) cases. Therefore, in ponderomotive acceleration, the energy spectral index naturally anti-correlates with the particle energy gain (and therefore the luminosity when converted into gamma rays).

On the other hand, the recent wakefield acceleration mechanism (Ebisuzaki & Tajima 2014a) has been suggested of the genesis of highest energy cosmic rays accelerated via wakefields generated by the Alfven shock emanated from the jet from an AGN accretion disk disruptions. It has an embedded feature of accelerating both protons (ions) as well as electrons simultaneously. Moreover, it has built-in characteristics of the following. While the Fermi mechanism is fundamentally stochastic (Fermi 1954), the current mechanism is based on the coherent baseline process with the relativistic coherence, though there are elements that bring in stochastic processes that overlay the coherent mechanism. High-energy electrons accelerated by this mechanism in its purest form (dominated by nearly one dimensional collimation along the axis of the blazar) have the power-law spectrum of energy with photon index of 2. If there are less ideal or less robust regime of its operation, the power index would rise above 2. When the wakefield generation is most robust, naturally the luminosity is also highest. The acceleration process has inherent rapid time scales. The shortest time variation is about 100 seconds, reflecting the Alfven wave structure, the next time hierarchy has days-weeks associated with the occurrence of the accretion disruption interval, and the longest time scale corresponds to the acceleration time of the highest energy cosmic rays $(1 - 10^3$ years). This last time scale is primarily for protons. For electrons with much lighter mass, the acceleration time scale may be in the range from 100 seconds to weeks, in other words, the first and second time scales, though the time structure depends on the detailed acceleration configuration. Although the gamma-ray luminosity integrated over $4\pi$ is on the order of $10^{41}$ erg s$^{-1}$ for a black hole of $10^8$ $M_\odot$ and normalized accretion rate of $0.1 M_\odot/\text{yr}$, the boosted-apparent luminosity reaches $10^{44} - 10^{45}$ erg s$^{-1}$, depending on the $\gamma$-factor of the jet. This is within a few orders of magnitude of the observed gamma-ray luminosities of blazars. For example, blazar 3C 454.3 has a bolometric luminosity from 0.1 to 100 GeV of $4.1 \times 10^{48}$ erg s$^{-1}$ (Nolan et al. 2012). The episodic dynamics of the magnetic eruption of a black hole's accretion disk, along with the associated intense disruption of their jets was studied via three-dimensional general-relativistic magnetohydrodynamics in Mizuta et al. (2017).

## 3. SYNCHROTRON TO INVERSE COMPTON ACCELERATION

In this section, we briefly review how accelerated electrons lead to the observed gamma-ray spectrum. For the majority of blazars the gamma-ray emission can
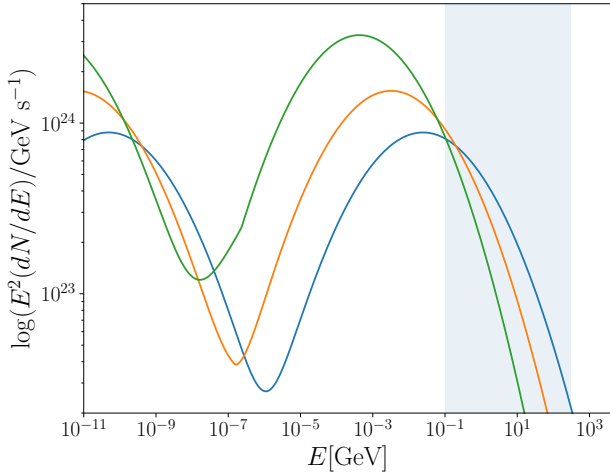
FIG. 1.— Shown is a standard blazar sequence model for a typical blazar SED, based on Inoue & Totani (2009). The energy band of our observations is indicated by the filled blue box. As can be seen in this illustration, a higher luminosity (green curve) relative to a lower luminosity (blue curve) would correspond to a photon spectral index closer to $\Gamma = 2$. This is what we dub the "internal blazar sequence." A spectral index of $\Gamma = 2$ is horizontal on this plot. The orange curve represents the possibility of observing the photon spectrum that is more closely-tied to the intrinsic electron spectrum at higher energies than the inverse Compton peak intensity.

be well described by the process of synchrotron self-Compton (Longair 2011). This is the process by which synchrotron photons, produced in great abundance by high-energy electrons in the magnetic field of the blazar jet, are up-scattered by inverse-Compton collisions by these same electrons. Photons emitted by the accretion disk may also be up-scattered. The intensity spectrum has a characteristic double-humped feature where the inverse-Compton high energy gamma-ray emission is an inverse-Compton processed up-scattering reflection of the lower-energy emission (Fossati et al. 1997, 1998; Donato et al. 2001). A model spectrum of this variety is shown in Fig. 1. Here we review the basic physics of the synchrotron mechanism that feeds into the synchrotron self-Compton process, based on Longair (2011). The high-energy gamma-ray spectrum of blazars may also have contributions from high energy hadronic cosmic rays (Takami et al. 2013), though synchrotron self-Compton models in general do a superior job in explaining the broad blazar SED.

The primary energy flux at a given frequency $\nu$, $J(\nu)$, peaks in synchrotron emission at a characteristic frequency,

$$\nu_c \approx \gamma^2 \nu_g = \left( \frac{E^2}{m_e c^2} \right)^2 \nu_g \,, \tag{1}$$

for an electron of energy $E$, where the gyrofrequency is $\nu_g = eB/2\pi m_e$. The energy radiated in frequency interval $(\nu, \nu + d\nu)$ is,

$$J(\nu)d\nu = \left( -\frac{dE}{dt} \right) N(E)\, dE \,, \tag{2}$$

where the electron population has a number distribution as $N(E)dE = \kappa E^{-p} dE$. The energy loss rate for synchrotron radiation is,

$$-\left( \frac{dE}{dt} \right) = \frac{4}{3}\sigma_T c \left( \frac{E}{m_e c^2} \right)^2 \frac{B^2}{2\mu_0} \,, \tag{3}$$

and the energy flux is,

$$J(\nu) \propto \kappa B^{(p+1)/2} \nu^{-(p-1)/2} \,. \tag{4}$$

So, the emitted synchrotron spectrum $J(\nu) \propto \nu^{-a}$ is related to the intrinsic electron energy spectrum $p$ as $a = (p-1)/2$. However, the synchrotron emission undergoes self-absorption that alters the observed spectrum. This is due to the limitation that no region can emit incoherent radiation at an intensity greater than that of a black-body at its thermodynamic temperature. At low enough frequencies, the "brightness temperature" of the radiation approaches the "thermal" temperature of the radiating electrons. The *brightness temperature* is derived from that of a black-body, but is applicable to any emission process, and is defined as $T_b = (\lambda^2/2k)(S_\nu/\Omega)$, where $\lambda$ is the emission wavelength, $S_\nu$ is the flux density, and $\Omega$ is the solid angle the source subtends at the observer. The effective temperature of the electrons must match the brightness temperature, and therefore the observed intensity must be (Longair 2011),

$$S_\nu \propto \frac{\nu^{5/2}}{B^{1/2}} \,. \tag{5}$$

Therefore, a pure synchrotron self-absorption spectrum is a rising spectrum as $I \propto \nu^{5/2}$ and then falls over to the inherent synchrotron spectrum $I \propto \nu^{-(p-1)/2}$. The inverse Compton spectrum reflects that since in that case the energy of the up-scattered photons are $\hbar\nu = (4/3)\gamma^2\hbar\nu_0$, where $\nu_0$ is the originating photon's frequency.

There is one basic conclusion regarding the relation of the observed photon spectrum in gamma rays or radio frequencies: the observed energy spectrum could reflect the originating spectrum well above the synchrotron peak where $I_\nu \propto \nu^{-(p-1)/2}$, but that is not necessarily achieved in the given observational window, which could lie below the synchrotron peak, near it, or above it, but still in its spectrally curved region.

For an example blazar temporal sequence, we adopt the SED spectral model first quantified in Inoue & Totani (2009). However, any smoothly curved spectrum is likely sufficient, and we make no effort to fit a model. We show for first time that, for the case of low-synchrotron peak blazars we observe, the temporal variation of flux is consistent with a given blazar shifting in flux and bolometric luminosity along such a temporal blazar sequence. Our results and others of observed gamma-ray spectra appear to be near the intensity peak (overturn) of the inverse Compton emission, where $a = 2$, and so are not likely reflective of the source electron spectra. Higher energy observations, such as with the High Altitude Water Cherenkov (HAWC) gamma-ray observatory (Lauer & Younk 2016), as well as temporal observations, may say more about the intrinsic electron spectra.

## 4. METHOD

Throughout our analysis, we use Fermi Tools version `v9r33p0` to study Fermi LAT Pass 7 reprocessed data

| Blazar name | Optical class | SED class |
|---|---|---|
| 3C 454.3 | FSRQ | LSP |
| PKS 1510-08 | FSRQ | LSP |
| PKS 1502+106 | FSRQ | LSP |
| PKS 0537-441 | BL Lac | LSP |
| 4C +21.35 | FSRQ | LSP |
| PKS 0426-380 | BL Lac | LSP |
| Mkn 421 | BL Lac | HSP |
| 3C 279 | FSRQ | LSP |
| 3C 66A | BL Lac | ISP |
| PKS 2155-304 | BL Lac | HSP |
| PKS 0454-234 | FSRQ | – |
| PKS 0727-11 | FSRQ | – |

taken from August 2008 to February 2015 (approximately 85 months of data), using both front and back-converting, SOURCE-class photons. We select the twelve blazars with the highest photon flux from the Fermi LAT second AGN catalog (Ackermann et al. 2011). These blazars are listed in Table 1, along with their optical and SED class. For each blazar, gamma rays within a circular region of interest (ROI), 7 degrees in radius and centered on the blazar, are selected, as was done in Abdo et al. (2010b). We use photons with energies between 100 MeV and 300 GeV, and apply the standard cuts recommended by the Fermi collaboration to ensure data quality (zenith angle < 100 degrees, DATA_QUAL = 1, LAT_CONFIG = 1).

Our model for each of the twelve regions of interest is composed of all of the sources identified in the LAT 4-year point source (3FGL) catalog, along with the recommended diffuse emission models associated with the Galactic emission (gll_iem_v05_rev1) and the isotropic background (iso_source_v05) which accounts for the contributions from both the extragalactic background and cosmic ray contamination. Despite the fact that a number of blazars in this analysis display significant curvature in their spectra over wide ranges in energy, we employ a relatively narrow energy window. We adopt simple power-law model consisting of two free parameters, a normalization factor $N_0$ and spectral index $\Gamma$, for the spectrum of each blazar. The convention used in this paper is that the spectral index $\Gamma$ should be taken to be positive, so that the photon flux is proportional to $E^{-\Gamma}$, where $E$ is the energy. This is done to provide a convenient means of characterizing the relative hardness or softness of the photon spectrum, which is the primary goal of this analysis.

Once we construct a model for the ROI around a particular blazar, we use standard maximum likelihood methods to fit the free parameters of the various gamma-ray sources in our model. To determine which parameters to vary, we make use of the quantity TS, which is defined as twice the difference in log-likelihood between a model with and without a particular source, i.e. TS = $2\Delta \ln(\mathcal{L})$ (TS = 25 corresponds to an approximate detection significance of about $5\sigma$ for point sources). We then determine the variability of the photon flux and spectral index over time for each of the twelve blazars by dividing up the full time range into time bins and refitting the parameters for the source of interest, leaving all other sources in the ROI fixed to their best fit values found from the

full time range. This procedure, which makes use of the LAT analysis scripts quickAnalysis, quickLike, and quickCurve, are described in more detail below.

1. First, a binned likelihood analysis of the region is performed using photons from the full time range. This is referred to as the DC analysis (analogous to "direct current").

   - The raw photons file is filtered and processed according to the previously described specifications for each blazar using the quickAnalysis tool.

   - The model file for the ROI is generated using the user contributed tool make3FGLxml.py and then changing the spectral shape of the source of interest to a power law.

   - The parameters for sources with TS > 25 are left free. Sources with 4 < TS < 25 have their spectrum fixed to their 3FGL values but their normalizations are left free. Finally, sources with TS < 4 have all of their parameters fixed to their 3FGL values.

   - A standard binned maximum likelihood analysis is performed using the quickCurve tool to find the best-fit values for all of the remaining free parameters in the model. This model is called the DC model.

2. Next, the full time range is divided up into time bins and a separate unbinned likelihood analysis is performed for each time bin. This is referred to as the AC analysis (analogous to "alternating current").

   - The entire time range is divided into equally sized time bins of 7.9 days, resulting in a total of 300 time bins. Though there may be temporal variation on time scales smaller than this, our timing resolution is limited by the detection significance of the source of interest, and we are unable to reliably probe time scales significantly shorter than about a week.

   - All of the relevant analysis files to perform an unbinned likelihood analysis for each time bin are generated using the quickCurve tool, using the same specifications as in step 1.

   - The DC model from step 1 is copied, but all of the sources except for the source of interest are fixed to their best fit values from the DC analysis. Only the normalization factor and spectral index of the source of interest are left free.

   - An unbinned maximum likelihood analysis is performed in order to determine the best-fit values for the normalization and spectral index of the source of interest.

3. Step 2 is repeated once again, but using time bins that are larger by a factor of six (about 47.5 days), resulting in 50 time bins instead of 300. This has the effect of increasing the detection significance of the source of interest in each time bin at the cost of losing sensitivity to short time-scale variations.
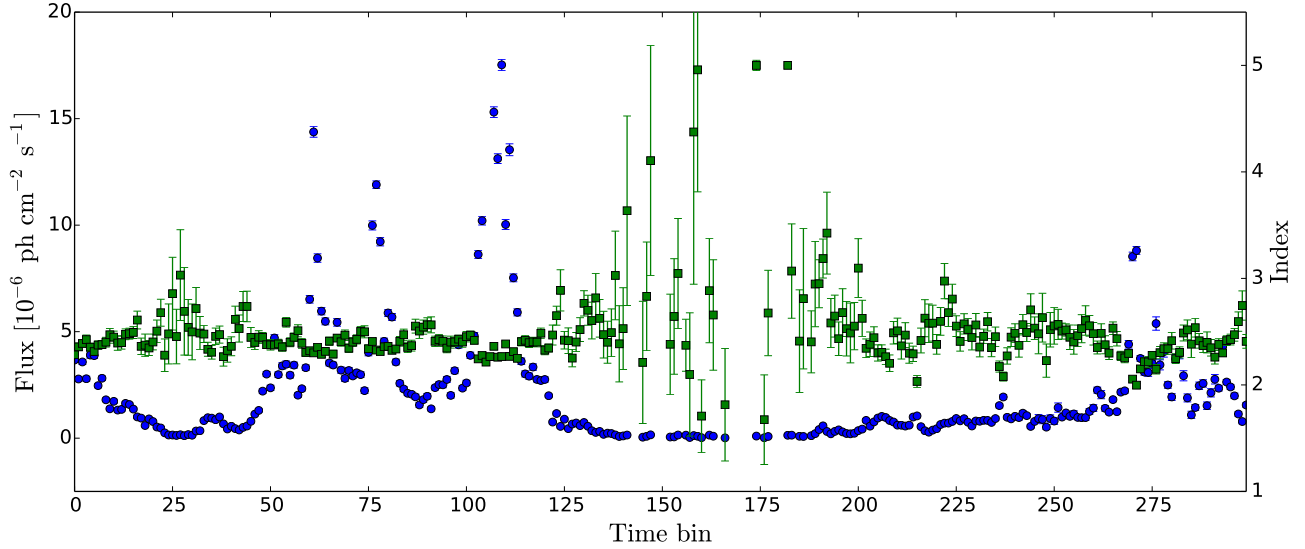
FIG. 2.— Shown are the flux (blue circles, left axis) and spectral index (green squares, right axis) for 3C 454.3 in 300 time bins of 7.9 days duration. An anti-correlation can be seen: the peaks in flux correspond to dips in the spectral index and vice versa.

TABLE 2
LIST OF BLAZARS AND THE PEARSON CORRELATION COEFFICIENT BETWEEN THEIR PHOTON FLUX AND SPECTRAL INDEX, ALONG WITH THE CORRESPONDING APPROXIMATE P-VALUE FOR THE 50 TIME BIN ANALYSIS.

| AGN name | r | p-value | $\sigma^2_{NXS,flux}$ | $\sigma^2_{NXS,index} \times 10^{-2}$ |
|---|---|---|---|---|
| 3C 454.3 | -0.416 | $2.7 \times 10^{-3}$ | $2.44 \pm 0.010$ | $1.44 \pm 0.14$ |
| PKS 1510-08 | -0.441 | $1.3 \times 10^{-3}$ | $0.99 \pm 0.012$ | $0.04 \pm 0.03$ |
| PKS 1502+106 | -0.681 | $5.1 \times 10^{-8}$ | $1.306 \pm 0.026$ | $0.42 \pm 0.40$ |
| PKS 0537-441 | -0.379 | $6.7 \times 10^{-3}$ | $0.381 \pm 0.013$ | $0.38 \pm 0.09$ |
| 4C +21.35 | -0.491 | $3.0 \times 10^{-4}$ | $1.28 \pm 0.017$ | $0.68 \pm 0.12$ |
| PKS 0426-380 | -0.254 | $7.5 \times 10^{-2}$ | $0.34 \pm 0.013$ | $0.50 \pm 0.10$ |
| Mkn 421 | -0.065 | $6.5 \times 10^{-1}$ | $0.165 \pm 0.008$ | $0.03 \pm 0.03$ |
| 3C 279 | -0.265 | $6.3 \times 10^{-2}$ | $0.82 \pm 0.016$ | $0.23 \pm 0.07$ |
| 3C 66A | 0.104 | $4.7 \times 10^{-1}$ | $0.21 \pm 0.016$ | $-1.49 \pm 0.04$ |
| PKS 2155-304 | 0.680 | $5.6 \times 10^{-8}$ | $0.40 \pm 0.023$ | $0.52 \pm 0.12$ |
| PKS 0454-234 | -0.587 | $7.4 \times 10^{-6}$ | $0.34 \pm 0.013$ | $0.49 \pm 0.12$ |
| PKS 0727-11 | -0.145 | $3.1 \times 10^{-1}$ | $0.31 \pm 0.019$ | $1.20 \pm 0.28$ |

## 5. RESULTS

We find that all blazars displayed significant temporal variation in both their flux and spectral index. Fig. 2 shows the variation of the flux and spectral index for blazar 3C 454.3 over the 300 time bins. For nine out of the twelve blazars studied in this analysis, we observe a weak to moderate anti-correlation between the flux of the blazar and its spectral index. Six of these are statistically significant (*p*-value ¡ 0.05). In other words, for most of the blazars, we observe the same "harder when brighter" effect that has been noted in other analyses (Abdo et al. 2010b). This can be seen in Fig. 2, as the peaks in flux correspond to dips in the spectral index and vice versa.

This anti-correlation can be seen more clearly in Fig. 3 which shows the spectral index vs. flux for nine of the blazars in the 50 time bin analysis. The anti-correlation is seen in both the 50 time bin analysis and the 300 time-bin analysis. The Pearson correlation coefficients are shown in Table 2 along with their corresponding approximate *p*-values. Three blazars do not exhibit this anti-correlation (Fig. 4). Two of the three, Mkn 421 and PKS

2155-304, are high synchrotron peak (HSP) BL Lacs, and the third blazar, 3C 66A, is an intermediate synchrotron peak (ISP) BL Lac. This same pattern of flat-spectrum radio quasars (FSRQs) and low synchrotron peak (LSP) BL Lacs displaying the anti-correlation and HSP BL Lacs not exhibiting the effect was previously noted in Abdo et al. (2010b), although they also note that ISP-BLLacs tend to display it in some cases. Possible explanations for this behavior will be elaborated on further in Section 6.

We estimate the intrinsic source variance by calculating the excess variance $\sigma^2_{XS}$, as described in Vaughan et al. (2003). The excess variance is the variance after subtracting the contribution from measurement errors such as Poisson noise and is defined as,

$$\sigma^2_{XS} = S^2 - \overline{\sigma^2_{err}}, \qquad (6)$$

where $S^2$ is the sample variance of $N$ data points,

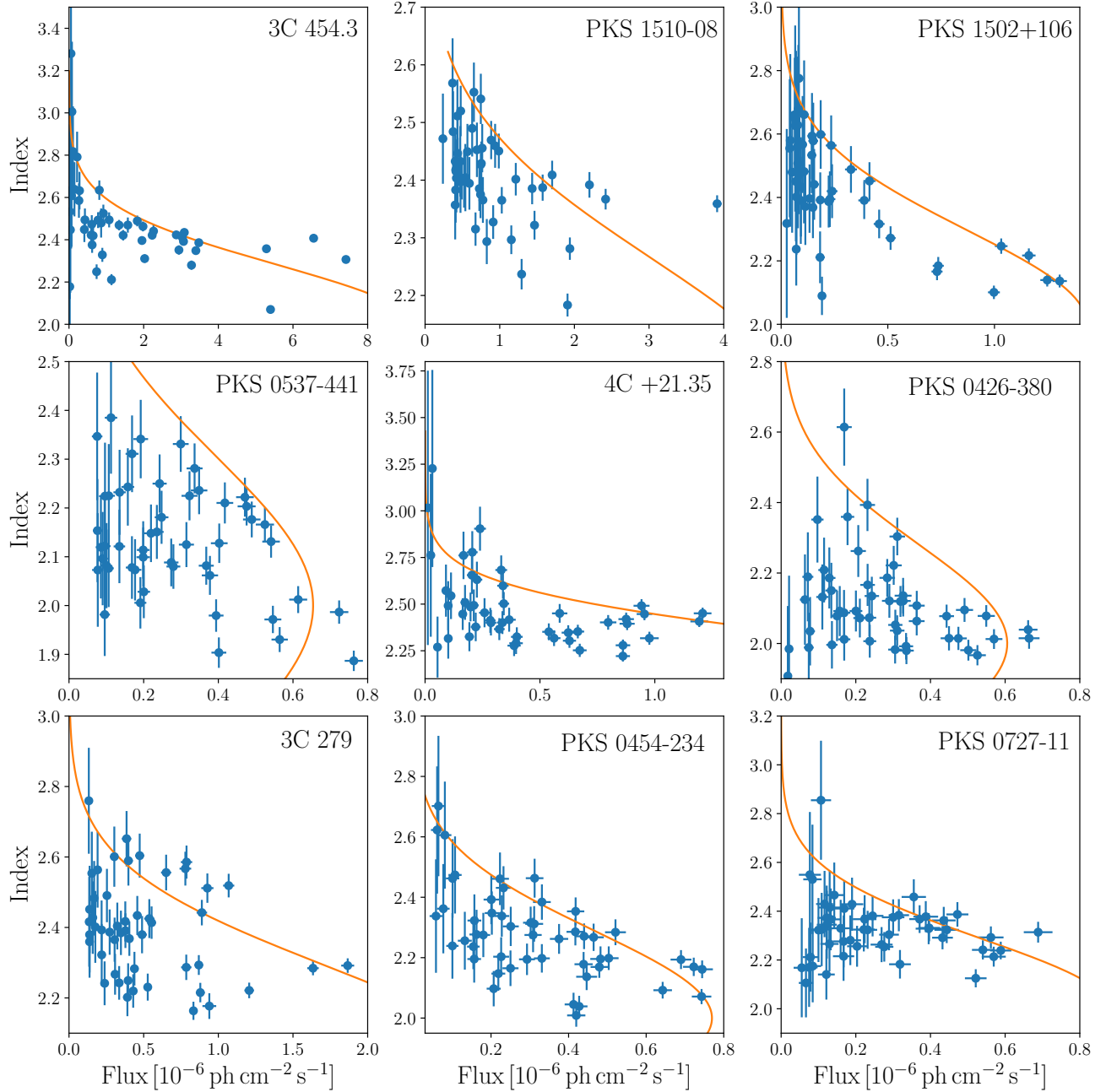$$S^2 = \frac{1}{N-1} \sum_{i=2}^{N} (x_i - \overline{x})^2, \qquad (7)$$

FIG. 3.— Shown here are the flux vs. index for the nine the blazars analyzed in the 50 time bin analysis that exhibit the flux-spectral anti-correlation attributable to the inverse Compton up-scattering of synchrotron photons. The orange curve is the slope from the blazar SED model shown in Fig. 1, which is not fit to the data, yet corresponds well with the observations. This is what we dub the "internal blazar sequence."

and $\overline{\sigma_{err}^2}$ is the mean square error,

$$\overline{\sigma_{err}^2} = \frac{1}{N} \sum_{i=1}^{N} \sigma_{err,i}^2. \qquad (8)$$

The normalized excess variance is given by $\sigma_{NXS}^2 = \sigma_{XS}^2 / \overline{x}^2$, and the error on $\sigma_{NXS}^2$ was calculated according

to,

$$err(\sigma_{NXS}^2) = \sqrt{\left(\sqrt{\frac{2}{N}} \cdot \frac{\overline{\sigma_{err}^2}}{\overline{x}^2}\right)^2 + \left(\sqrt{\frac{\overline{\sigma_{err}^2}}{N}} \cdot \frac{2F_{var}}{\overline{x}}\right)^2}, \qquad (9)$$

as given in Vaughan et al. (2003). Here, $F_{var}$ is the fractional root mean square (rms) variability amplitude and is simply the square root of the normalized excess variance, i.e., $F_{var} = \sqrt{\sigma_{NXS}^2}$. The measured values for normalized excess variance of the photon flux $\sigma_{NXS,flux}^2$
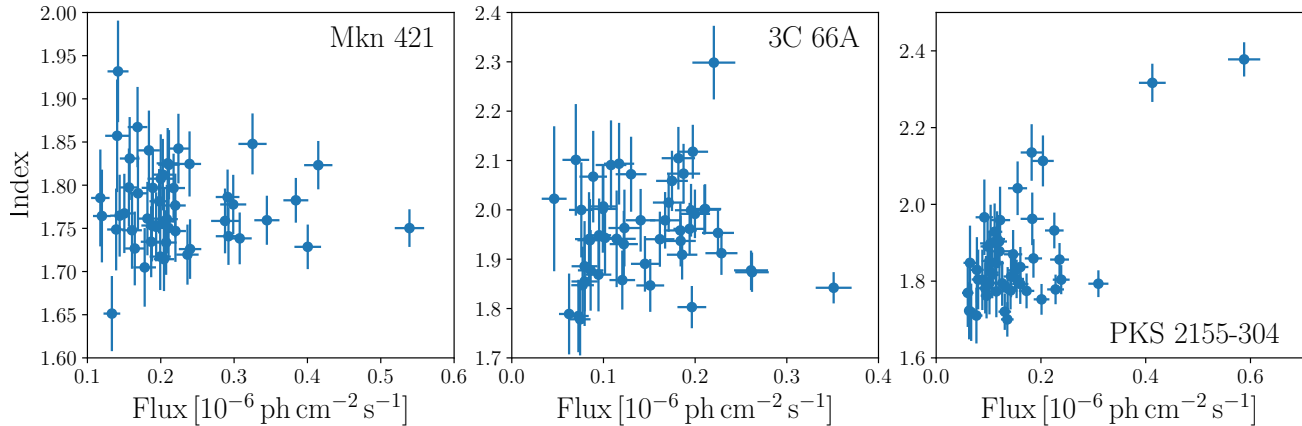
FIG. 4.— Shown here are the flux vs. index for three blazars not exhibiting the flux-spectral index anti-correlation. Unlike the LSPs in Fig. 3, two of the three, Mkn 421 and PKS 2155-304, are HSP-BLLacs, and the third blazar, 3C 66A, is an ISP BL Lac. The pattern of FSRQs and LSP BL Lacs displaying the anti-correlation and HSP BL Lacs not exhibiting the effect was previously noted in Abdo et al. (2010b). ISP-BLLacs tend to display it in some cases. We discuss these differentiated cases in Section 6.

and for the spectral index $\sigma^2_{NXS,index}$ are also shown in Table 2.

## 6. DISCUSSION

We have clearly established the anti-correlation between the luminosity of gamma rays from blazars and their spectral index. The anti-correlation is clearly consistent with a shift from off-peak to peak portions of the blazar spectra, as shown in Figs. 1 and 3, for the case of LSP BL-Lacertae blazars. This is the first time that a temporal-sequence model has been applied to show the origin of the spectral-flux anti-correlation.

We followed in this study the earlier observations by Abdo et al. (2010b) and Abdo et al. (2010c). In our work, we scan different blazars with different values of flux and index, as in these prior analyses. When they surveyed different blazars, they showed different rise times of the brightening and the lowering of the spectral index as well as the interval times between such bursts of luminosity surge. The rise (and fall) times in most cases scale with the interval times between the events, i.e., the longer the rise time of the burst is, the longer the interval is.

Even though the time scale varies over orders of magnitude, this phenomenon is universal. In fact, Ebisuzaki & Tajima (2014a) predicts that all these events are universally based on the wakefield excitation in the jets sharing the common acceleration mechanism, which is the basis for this universality.

We note that the observed phenomenon of the anti-correlation between the luminosity and the spectral index remains manifest, regardless of the mentioned rise time and interval time scales. According to the theory of Ebisuzaki & Tajima (2014a), the periods of both the rise time and the interval time scale are proportional to the mass of the central AGN mass (Ebisuzaki & Tajima 2014a). In other words, though an AGN with different mass may show a proportional time scale of variability, these phenomena are common and the luminosity-index anti-correlation is one of the strongest evidence for the universal nature of acceleration mechanism. It should be further noted that not only these universal phenomena are expected and/or observed (by theory and observa-

tion) of blazars, but also these should be expected for microquasars with much smaller masses, as predicted in Ebisuzaki & Tajima (2014b). Therefore, it is encompassing several orders of a wide range of masses from microquasars to most massive AGNs. From this discussion, we now suggest the following prediction: from the period time scale of the blazar gamma ray emissions, we can surmise the mass of the central object of the particular blazar (and microquasar). Therefore, the intrinsic luminosity of blazars, though collective of apparent luminosity depend on the observational conditions, can also tell us about the mass of the central object, as they also scale proportional to the mass (Ebisuzaki & Tajima 2014a,b).

Our own analysis (Fig. 2) and subsequent analyses also underline the following picture: when the gamma-ray emission from blazars increases, the gamma-ray spectrum tends to become harder. This observed tendency, which is in agreement with previous observation (Abdo et al. 2010b), is consistent with a temporal SED sequence, shifting emission from near peak to peak inverse Compton emission flux. Higher energy observations, such as with the HAWC observatory, may be able to probe the intrinsic electron spectrum to test its consistency with the wakefield acceleration in the jets. For HSP and ISP blazars, we do not see the anti-correlation as we had for LSP blazars with lower-energy synchrotron peaks. This is is due to the fact that, for HSP and ISP, the spectral peak is within the energy window, not exhibiting the monotonic SED sequence anti-correlation. In addition, several of our tested HSP and ISP blazars exhibit no significant curvature in their spectra (Abdo et al. 2010d).

The episodic disk instability launches the energetic Alfven shocks, and their subsequent electromagnetic pulsations, such as in the Ebisuzaki-Tajima mode (Ebisuzaki & Tajima 2014a). This model naturally points to a localized source (as observed in Abdo et al. 2010b; Albert et al. 2007). Such localized emission of gamma-rays (arising from accelerated electrons) and expected localized acceleration of ions from such locations are integral properties of the wakefield acceleration mech-

anism. Furthermore, the wakefield acceleration of ultra-high energy cosmic-ray ions has the unique property of localized gamma-ray emission, while the Fermi acceleration mechanism relies on a diffuse site and therein lies the difficult issue of stochastic genesis. In addition to the above issue of super-high energetic genesis of cosmic rays (and associated gamma-ray bursting emissions), the wakefield acceleration mechanism should be a natural candidate for more compact gamma-ray emission from, e.g., Crab Nebula (Buehler et al. 2012; Abdo et al. 2011), and the microquasar Cyg. X-1 (Nowak et al. 2012;

Ebisuzaki & Tajima 2014b). With continued observations of high-energy gamma-ray emission from blazars, especially those at the highest energies, the underlying emission processes and acceleration mechanisms may be further revealed.

REFERENCES

Abdo, A. A. et al. 2010a, Astrophys. J., 722, 520, arXiv:1004.0348 [astro-ph.HE]
—. 2010b, Astrophys.J., 710, 1271, arXiv:1001.4097 [astro-ph.HE]
—. 2010c, Astrophys.J., 715, 429, arXiv:1002.0150 [astro-ph.HE]
—. 2010d, Astrophys.J., 716, 30, arXiv:0912.2040 [astro-ph.CO]
Abdo, A. A. et al. 2011, Science, 331, 739, arXiv:1011.3855 [astro-ph.HE]
Ackermann, M. et al. 2011, ApJ, 743, 171, arXiv:1108.1420 [astro-ph.HE]
Aharonian, F. 2007, Astrophys.J., 664, L71, arXiv:0706.0797 [astro-ph]
Albert, J., Aliu, E., Anderhub, H., Antoranz, P., Armada, A., et al. 2007, Astrophys.J., 669, 862, arXiv:astro-ph/0702008 [astro-ph]
Aleksic, J. et al. 2011, Astrophys.J., 730, L8, arXiv:1101.4645 [astro-ph.HE]
Ashour-Abdalla, M. et al. 1981, Phys. Rev., A23, 1906
Buehler, R., Scargle, J. D., Blandford, R. D., Baldini, L., Baring, M. G., Belfiore, A., Charles, E., Chiang, J., D'Ammando, F., Dermer, C. D., Funk, S., Grove, J. E., Harding, A. K., Hays, E., Kerr, M., Massaro, F., Mazziotta, M. N., Romani, R. W., Saz Parkinson, P. M., Tennant, A. F., & Weisskopf, M. C. 2012, ApJ, 749, 26, arXiv:1112.1979 [astro-ph.HE]
Chen, L.-E., Li, H.-Z., Yi, T.-F., Zhou, S.-B., & Li, K.-Y. 2013, Research in Astronomy and Astrophysics, 13, 5
Donato, D., Ghisellini, G., Tagliaferri, G., & Fossati, G. 2001, A&A, 375, 739, arXiv:astro-ph/0105203 [astro-ph]
Ebisuzaki, T. & Tajima, T. 2014a, Astroparticle Physics, 56, 9, arXiv:1306.0970 [astro-ph.HE]
—. 2014b, Eur. Phys. J. ST, 223, 1113
Edelson, R., Mushotzky, R., Vaughan, S., Scargle, J., Gandhi, P., Malkan, M., & Baumgartner, W. 2013, Astrophys. J., 766, 16, arXiv:1302.4445 [astro-ph.HE]
Edelson, R., Vaughan, S., Malkan, M., Kelly, B., Smith, K., Boyd, P., & Mushotzky, R. 2014, Astrophys. J., 795, 2, arXiv:1409.1613 [astro-ph.HE]
Fermi, E. 1954, ApJ, 119, 1

Fossati, G., Celotti, A., Ghisellini, G., & Maraschi, L. 1997, MNRAS, 289, 136, arXiv:astro-ph/9704113 [astro-ph]
Fossati, G., Maraschi, L., Celotti, A., Comastri, A., & Ghisellini, G. 1998, MNRAS, 299, 433, arXiv:astro-ph/9804103 [astro-ph]
Giannios, D., Uzdensky, D. A., & Begelman, M. C. 2009, MNRAS, 395, L29, arXiv:0901.1877 [astro-ph.HE]
Inoue, Y. & Totani, T. 2009, Astrophys. J., 702, 523, arXiv:0810.3580 [astro-ph]
Lauer, R. J. & Younk, P. W. 2016, in Proceedings, 34th International Cosmic Ray Conference (ICRC 2015): The Hague, The Netherlands, July 30-August 6, 2015, Vol. ICRC2015, 716, 1508.04479
Longair, M. S. 2011, High Energy Astrophysics (Cambridge University Press)
Marscher, A. P. et al. 2008, Nature, 452, 966
Mima, K., Tajima, T., & Hisegawa, A. 1991, in Nonlinear Dynamics in Particle Acceleration, ed. Y. H. Yoshikawa & T. Tajima, 27
Mizuta, A., Ebisuzaki, T., Tajima, T., & Nagataki, S. 2017, arXiv:1707.08799 [astro-ph.HE]
Nolan, P. L., Abdo, A. A., Ackermann, M., Ajello, M., Allafort, A., Antolini, E., Atwood, W. B., Axelsson, M., Baldini, L., Ballet, J., & et al. 2012, Astrophys.J.Suppl., 199, 31, arXiv:1108.1435 [astro-ph.HE]
Nowak, M. A., Wilms, J., Pottschmidt, K., & Markoff, S. 2012, Mem. Soc. Ast. It., 83, 202, arXiv:1107.2391 [astro-ph.HE]
Tajima, T. 2010, Proceedings of the Japanese Academy of Sciences, B86, 147
Tajima, T. & Dawson, J. M. 1979, Physical Review Letters, 43, 267
Takami, H., Murase, K., & Dermer, C. D. 2013, Astrophys. J., 771, L32, arXiv:1305.2138 [astro-ph.HE]
Tavecchio, F., Roncadelli, M., Galanti, G., & Bonnoli, G. 2012, Phys.Rev., D86, 085036, arXiv:1202.6529 [astro-ph.HE]
Vaughan, S., Edelson, R., Warwick, R. S., & Uttley, P. 2003, Mon. Not. Roy. Astron. Soc., 345, 1271, arXiv:astro-ph/0307420 [astro-ph]